Century-scale trends and seasonality in pH and temperature for shallow zones of the Bering Sea

Jan Fietzke[a,1], Federica Ragazzola[a,b,c], Jochen Halfar[d], Heiner Dietze[a], Laura C. Foster[b], Thor Henrik Hansteen[a], Anton Eisenhauer[a], and Robert S. Steneck[e]

[a]GEOMAR Helmholtz Centre for Ocean Research Kiel, 24148 Kiel, Germany; [b]Department of Earth Sciences, University of Bristol, Bristol, BS8 1RJ, United Kingdom; [c]Institute of Marine Sciences, University of Portsmouth, Eastney, Portsmouth, P04 9LY, United Kingdom; [d]Department of Earth Sciences, University of Toronto, Mississauga, ON, Canada L5L 1C6; and [e]School of Marine Sciences, University of Maine, Walpole, ME 04573

Edited by Taro Takahashi, Columbia University, Palisades, NY, and accepted by the Editorial Board January 28, 2015 (received for review October 6, 2014)

No records exist to evaluate long-term pH dynamics in high-latitude oceans, which have the greatest probability of rapid acidification from anthropogenic CO_2 emissions. We reconstructed both seasonal variability and anthropogenic change in seawater pH and temperature by using laser ablation high-resolution 2D images of stable boron isotopes ($\delta^{11}B$) on a long-lived coralline alga that grew continuously through the 20th century. Analyses focused on four multiannual growth segments. We show a long-term decline of 0.08 ± 0.01 pH units between the end of the 19th and 20th century, which is consistent with atmospheric CO_2 records. Additionally, a strong seasonal cycle (~0.22 pH units) is observed and interpreted as episodic annual pH increases caused by the consumption of CO_2 during strong algal (kelp) growth in spring and summer. The rate of acidification intensifies from –0.006 ± 0.007 pH units per decade (between 1920s and 1960s) to –0.019 ± 0.009 pH units per decade (between 1960s and 1990s), and the episodic pH increases show a continuous shift to earlier times of the year throughout the centennial record. This is indicative of ecosystem shifts in shallow water algal productivity in this high-latitude habitat resulting from warming and acidification.

ocean acidification | boron isotopes | isotope imaging | laser ablation ICP–MS | crustose algae

So far, about 30% of the anthropogenic carbon dioxide emissions have been taken up by the oceans (1, 2), which are one of the major reservoirs of the global carbon cycle. Since the mid-19th century, the carbon dioxide concentration in the atmosphere has increased to more than 390 μatm (3), well above the typical range reconstructed for the glacial/interglacial cycles (190–280 μatm) over the last 500,000 y. This increase in atmospheric CO_2 has shifted the carbonic acid equilibrium in seawater, resulting in a pH decrease (ocean acidification) lowering the carbonate ion concentration. Over the last ~150 y, the global average surface water pH has declined by about 0.15 pH units (2) and is expected to have further decreased by 0.3–0.4 pH units by the year 2100 (4). This is expected to trigger major shifts in marine ecosystems, challenging marine calcifiers' ability to form carbonate hard substrate as a consequence of a lowered calcium carbonate saturation state (4–6). This reduction of saturation (i.e., increase in solubility) is a direct consequence of the lowered carbonate ion concentration. Compared with this, the weak increase in saturation from rising temperatures (ocean warming) is almost negligible (7). Recent research on future changes of marine ecosystems has largely focused on laboratory-based culturing studies and mesocosm experiments (6, 8, 9). However, to make realistic predictions, additional information about past natural variability also needs to be obtained directly from long-lived calcifiers, which experienced a whole complexity of challenges within their natural habitats including pH variability (10).

Proxy-based reconstructions of ocean pH are commonly made by mass spectrometric determination [thermal ionization mass spectrometry (TIMS), secondary ion mass spectrometry (SIMS), and multi-collector (MC)–inductively coupled plasma (ICP)–MS] of $\delta^{11}B$ on discrete carbonate samples (11–14). Using these methods, long-term records of ocean pH variability have been established (15–17). However, these time series suffer from poor temporal resolution and do not resolve small-scale spatial heterogeneities of natural samples. High-resolution records are desired, as they allow for investigation of both short-term variability and long-term trends in pH. Furthermore, available pH proxy records focus on the tropics. At high latitudes, no such data are available, despite the fact that these regions naturally show a low carbonate saturation state and the highest CO_2 uptake due to the cold surface water temperature.

For the first time, to our knowledge, we apply the recently developed laser ablation–multi-collector–ICP–MS (LA–MC–ICP–MS) in situ method (18) as a microchemical imaging technique to provide a spatially and temporally highly resolved $\delta^{11}B$ record from a long-lived subarctic coralline alga. Crustose coralline red algae are long-lived marine organisms that form annually laminated high Mg–calcite structures (19). They are among the major calcifiers in shallow-water benthic communities from the tropics to polar regions (20, 21). The chemical composition of their skeleton is controlled by algal physiology responding to the environmental parameters (e.g., light, nutrients, temperature, pH) (22, 23). Coralline algae have received widespread attention as temperature proxy archives on weekly to multicentennial time scales (19, 24, 25).

For this study, we used a sample (Fig. 1) of the alga *Clathromorphum nereostratum* Lebednik, collected alive at 10 m

Significance

Increasing atmospheric CO_2 concentrations are potentially affecting marine ecosystems twofold, by warming and acidification. The rising amount of CO_2 taken up by the ocean lowers the saturation state of calcium carbonate, complicating the formation of this key biomineral used by many marine organisms to build hard parts like skeletons or shells. Reliable time-series data of seawater pH are needed to evaluate the ongoing change and compare long-term trends and natural variability. For the high-latitude ocean, the region facing the strongest CO_2 uptake, such time-series data are so far entirely lacking. Our study provides, to our knowledge, the first reconstruction of seasonal cycle and long-term trend in pH for a high-latitude ocean obtained from 2D images of stable boron isotopes from a coralline alga.

Author contributions: J.F. designed research; J.F. and F.R. performed research; J.F. contributed new analytic tools; J.H. and R.S.S. performed fieldwork and sample collection; J.F., F.R., and H.D. analyzed data; and J.F., F.R., J.H., H.D., L.C.F., T.H.H., A.E., and R.S.S. wrote the paper.

The authors declare no conflict of interest.

This article is a PNAS Direct Submission. T.T. is a guest editor invited by the Editorial Board.

[1]To whom correspondence should be addressed. Email: jfietzke@geomar.de.

This article contains supporting information online at www.pnas.org/lookup/suppl/doi:10.1073/pnas.1419216112/-/DCSupplemental.

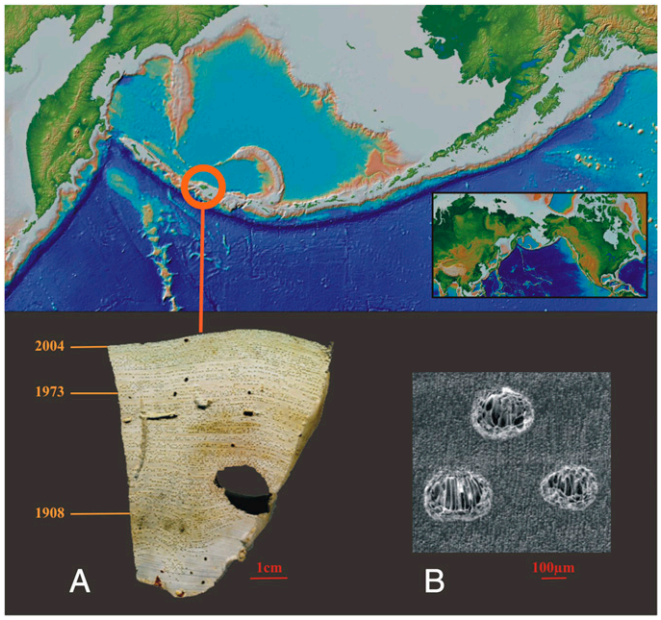

Fig. 1. *C. nereostratum* sample from Attu Island, Alaska. (*A*) Overview image of the sample including reference dates (29); lines of dark spots are conceptacle cavities. (*B*) Secondary Electron (SE) image of reproductive structures (conceptacles).

water depth off the eastern coast of Attu Island (Massacre Bay at Murder Point, Attu, Aleutian Islands—N 52° 47.787, E 173° 10.796) in August 2004. The local habitat is ecologically dominated by an annually growing kelp species (Dragon kelp, *Eualaria fistulosa*) being the main primary producer. The coastal waters of Attu Island are free of ice the whole year round [annual range, 2.2–10.5 °C, based on Extended Reconstructed Sea Surface Temperature (ERSST) v2] (26). The steep slopes of the Aleutian Island chain create a dynamic oceanographic environment (including upwelling), featuring the Alaskan Stream as the main current system south of the islands. This strong, westward boundary current transports relatively warm nutrient-rich, low-salinity (~32 psu) water passing through the gaps between the Aleutian Islands. It forms the Aleutian North Slope Current, an eastward current north of the island chain. One of the main inflows of the Alaskan Stream into the Bering Sea is Near Strait, located west of Attu Island (27, 28). The influence of the Pacific Decadal Oscillation on the multidecadal climate variability at the collection site has been reported in a previous publication (29).

The collected *C. nereostratum* specimen revealed a continuous growth record spanning from 1887 to 2004 (Fig. 1*A*), with growth rate averaging 370 µm/y (29). The age model has previously been established by counting annual growth increments and validated by uranium-series dating (29). The visual identification of annual growth increments is additionally aided by the annual formation of conceptacle cavities (reproductive structures; Fig. 1*B*). Starting in late summer, conceptacles develop in cavities partially formed by dissolution of the formerly precipitated calcite skeleton (30). The newly formed calcite structures within and surrounding the conceptacles may contain reprecipitated material and are morphologically and chemically distinct from the primary calcite. Hence, reliable proxy data can only be obtained from the primary calcite found in the vegetative thallus.

Mg/Ca ratios in different coralline algal species have previously been shown to be positively related to ambient seawater temperatures (24, 25, 31, 32). Mg/Ca-based temperature time series obtained from Mg/Ca electron microprobe (EMP) elemental mappings display a characteristic pattern related to the seasonal cycle in ambient water temperature (spatially biased by variable algal growth rates). Minima of 2–3 °C during winter and maxima of 10–11 °C mark the annual cycle recorded by the algal skeleton (Fig. 2). Element maps indicate that about 75% of the annually precipitated calcite is related to spring and summer

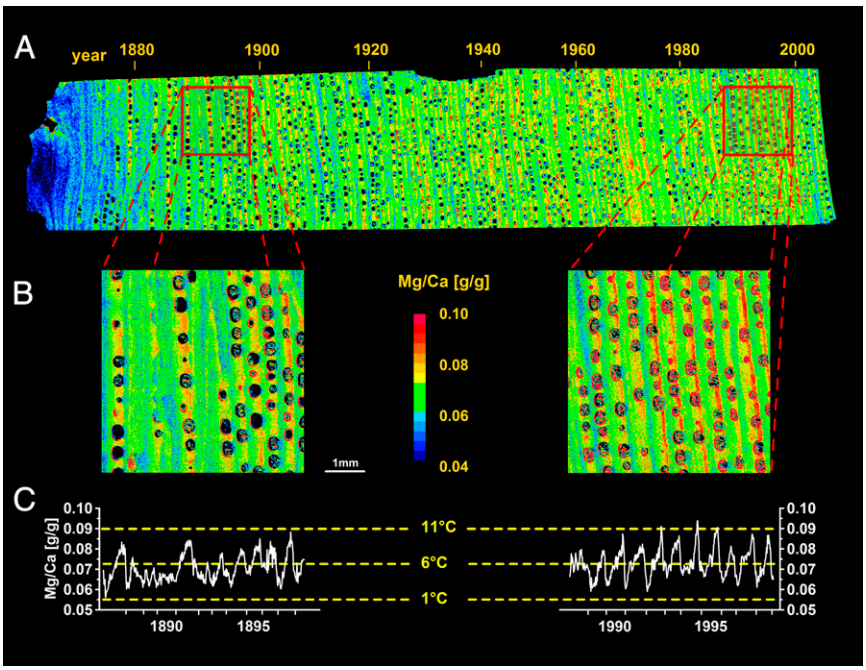

Fig. 2. EMP Mg/Ca elemental ratio maps used for temperature reconstruction. (*A*) Overview map of the whole sample (30 µm resolution) to examine long-term variability in Mg/Ca. (*B*) Subsample maps (5 µm resolution) from early-industrial (M-1887/97) and recent (M-1988/98) to examine intraannual variability in Mg/Ca. "M-years" designates the respective EMP map and the time interval covered. (*C*) Temperature reconstructed from Mg/Ca using data from *B*. Each data point of the time series represents average values of about 100 individual Mg/Ca data points from the original mappings (see *SI Appendix* for data treatment).

growth. The growth rate declines significantly by the end of summer. A likely explanation for this growth rate reduction is the beginning of conceptacle formation by the end of summer, as insolation declines and algal physiology shifts from growth to reproduction. It is also apparent from the elemental maps that conceptacle calcite contains significantly higher amounts of Mg than primary calcite and therefore must be excluded from the temperature reconstruction. Mean temperatures derived from Mg/Ca maps (Fig. 2) of 5.3 °C (M-1887/97; for sample denotation, see *Methods*) and 6.2 °C (M-1987/96) suggest a warming trend over the 100-y period.

Within the areas used for high-resolution EMP analysis, we acquired, to our knowledge, the first accurate and precise 2D images representing the variability of stable isotopes of boron ($^{11}B/^{10}B$) in natural samples using LA–MC–ICP–MS (18) at a resolution of 100 μm. This allows for the visualization of the spatial distribution of isotopic signatures in a complex sample (Fig. 3*A*; see *SI Appendix* for methods). In addition to cyclic intraannual $\delta^{11}B$ variability, the distinct composition of conceptacle calcite is apparent in the $\delta^{11}B$ images. This further highlights differences in the calcification process of both primary and secondary calcite.

C. nereostratum shows a large degree of variability in $\delta^{11}B$ values ranging from about 21 to 27. The low values are clearly associated with conceptacle areas (Fig. 3*A*). Using only data from primary calcite (*SI Appendix*), $\delta^{11}B$ averages in B-1888/94 are about 1–1.2 higher than in B-1989/96. The conversion of $\delta^{11}B$ into pH revealed a decline of 0.08 ± 0.01 pH units between B-1888/94 and B-1989/96, whereas the absolute boron-derived pH values are almost 0.7 pH units above the reasonable ambient seawater pH range in the Bering Sea. A comparable offset between $\delta^{11}B$-derived and ambient seawater pH has also been observed in other marine-calcifying organisms (e.g., corals) (33–36). It is interpreted as the result of the organism's physiological control on the calcifying fluid composition, up-regulating the pH relative to ambient seawater to provide more alkaline conditions to promote calcification (33–36). $\delta^{11}B$ is considered to represent the calcifying fluid pH (pH_{cf}). For corals, $\delta^{11}B$–pH calibration studies revealed the up-regulation being species-dependent, resulting in approximately half as strong a change in pH_{cf} relative to the external pH change (34). Nevertheless, different coral species show distinct sensitivities in the response to acidification and thus differ in their $\delta^{11}B$–pH relationship (i.e., their up-regulation potential) (33, 34).

No $\delta^{11}B$–pH calibration studies exist for coralline algae so far. Future studies will reveal if or to what extent the mentioned systematic found for corals can be transferred to coralline algae. A recently published study suggests the impact of seawater chemistry on the calcification is more direct for coralline algae than for corals (37). Consequently, we reconstruct pH_{cf} and its temporal changes from $\delta^{11}B$ in our algal sample. The observed drop of 0.08 ± 0.01 pH units is in good agreement with the expected shift in sea surface water pH from rising atmospheric pCO_2 levels (1900, ~295 μatm; 1990s, ~360 μatm). This suggests that boron isotope data derived from *C. nereostratum* accurately reflect long-term changes in seawater pH. It also implies the pH_{cf} in this algal species follows external pH more closely than reported for corals. Despite the long-term pH decline recorded by the coralline alga, potential negative impacts on annual skeletal growth rates of Bering Sea *C. nereostratum* corallines have not yet been observed (19).

Furthermore, the $\delta^{11}B$ images reveal cyclic variations (Fig. 3*B*), pointing to a distinct seasonal cycle of pH_{cf} and consequently seawater pH. When comparing the spatial distribution of both $\delta^{11}B$ and Mg/Ca maps, we find the highest boron isotopic values clearly preceding the annual peak in Mg/Ca. This suggests that the pH maximum occurs during late spring/early summer growth intervals (*SI Appendix*, *S4*). This seasonal cycle in $\delta^{11}B$ of up to 5 is observed for all 14 annual growth layers investigated in TS-1923/27, TS-1961/65, and TS-1989/92 (Fig. 4*D*). Less than 30% of the variability in $\delta^{11}B$ results from the influence of

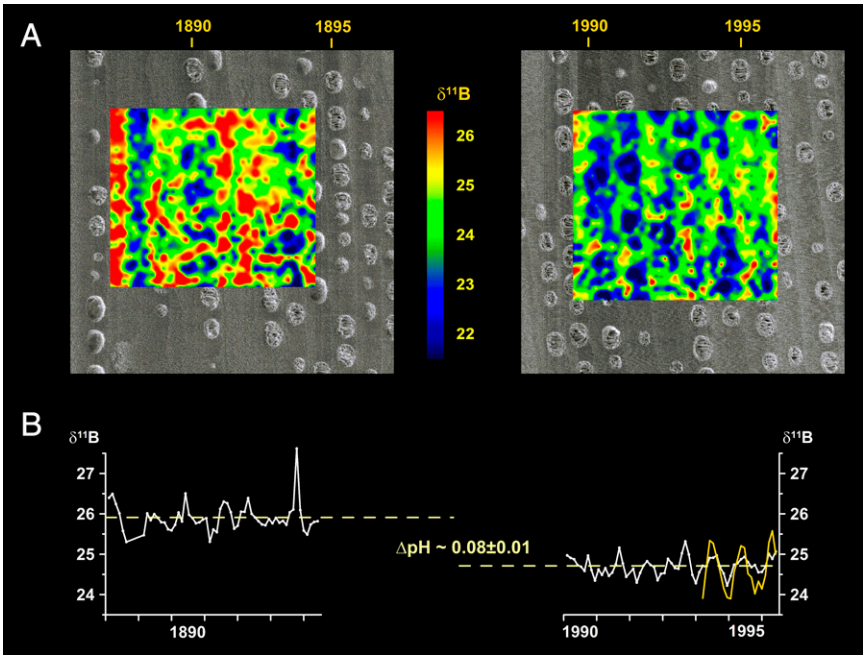

Fig. 3. Stable boron isotope ratio ($\delta^{11}B$) images acquired by LA–MC–ICP–MS used for pH reconstruction. (*A*) $\delta^{11}B$ images (100 μm resolution) displayed as overlays on secondary electron images from the EMP measurements (Fig. 2), referred to as B-1888/1894 and B-1989/96 in the text. (*B*) $\delta^{11}B$ time series showing a long-term decrease equal to 0.08 ± 0.01 pH units between the 1890s and 1990s in good agreement with atmospheric CO_2 records (see also *SI Appendix*). Additionally, a seasonal pH cycle of at least 0.1 pH units can be seen for the years 1994–1996 (yellow) using only data from the area least influenced by secondary calcite (see *SI Appendix* for data treatment).

temperature on the boric acid pK_B. The remaining signal trend corresponds to an average intraannual pH_{cf} variability of 0.22 ± 0.03, with the lowest values during winter and early spring and maxima during late spring and summer.

How does the observed algal annual pH data compare with what is known for the region? Attu Island is uninhabited and no time-series pH data have been made available to date. Hence, we are restricted to gridded climatological data. Using a recently published global seawater carbonate system dataset (38), we can estimate an annual pH signal for the open waters around Attu in the order of about 0.1 pH units (see details in *SI Appendix*, *S5* and Fig. S8), with the lowest pH calculated for January–March and highest values for July–October. This signal is less than half of what we have reconstructed from $\delta^{11}B$ in our algal sample. However, a significantly larger variability in pH is possible for the local coastal habitat where our *C. nereostratum* specimen had grown. As mentioned above, the local habitat is dominated by annually growing kelp, being the dominant primary producer. Kelp-dominated habitats are reported to be among the most productive ecosystems in the global ocean (39, 40). Starting in spring, these fast-growing macroalgae consume huge amounts of CO_2 for photosynthesis. As a consequence of depletion in dissolved CO_2 in the water, the carbonic acid equilibrium should shift toward higher pH values. Indeed, highly dynamic pH conditions have been reported for kelp-dominated habitats (41). Our observation of pH maxima occurring in spring/early summer agrees with the seasonality of kelp growth in this habitat, supporting the proposed effect.

Further support for the assumed higher pH dynamic linked to enhanced productivity is provided by the oceanographic environment, local topography, and remote-sensing data. As pointed out before, strong currents (Alaskan Stream in the South and Aleutian North Slope Current in the North), including the northward inflow into the Bering Sea through Near Strait, are the prominent hydrographic features close to Attu Island. The steep island slopes foster upwelling of nutrient-rich deeper water masses. A resulting enhanced productivity in coastal waters (so-called "island mass effect") has been reported for comparable environmental settings (42, 43). Satellite data of Chlorophyll a provide clear evidence for Attu Island being a productivity hotspot (for details, see *SI Appendix*, *S5* and Fig. S9). During summer, Chlorophyll a concentrations in coastal waters southeast off Attu Island exceed 2 mg/m^3, whereas in the open waters of this region 0.2–0.6 mg/m^3 is measured.

We therefore think a larger annual pH cycle than suggested by climatological data for open waters can be expected for this coastal habitat and is recorded by $\delta^{11}B$ in the calcite skeleton of *C. nereostratum*. Ultimately, $\delta^{11}B$–pH calibration studies are needed using specimens cultured under controlled conditions or free-living ones after data logger had been deployed in the natural habitat. For now, winter/early spring growth layers, when ambient water pCO_2 is equilibrated with the atmosphere (equating to $\delta^{11}B$ minima), are considered the most useful to assess the long-term pH trend. Indeed we find a gradual decline for the average internal pH minima (TS-1923/27, 8.683 ± 0.021; TS-1961/65, 8.660 ± 0.015; and TS-1989/92, 8.608 ± 0.020). This trend agrees well with the centennial 0.08 ± 0.01 reduction in pH obtained from B-1888/94 and B-1989/96 (Fig. 4*D*). Our results indicate an increase in the rate of acidification from -0.006 ± 0.007 pH units per decade (between 1920s and 1960s) to -0.019 ± 0.009 pH units per decade (between 1960s and 1990s), closely following the trend in atmospheric CO_2 concentration. With respect to relative pH change, our findings agree with the estimated global average surface water pH decline of 0.15 pH units over the last ~150 y (2). Nevertheless, due to the low water temperatures in this high-latitude ocean habitat, calcium carbonate saturation is significantly lower than in the tropical or temperate regions of the global oceans. Thus, any further saturation state reduction from lowered pH will potentially affect calcifying organisms stronger in the habitat investigated. Our results, however, are based on the four growth segments analyzed. Therefore, we cannot rule out interannual or interdecadal pH variability, on which future studies should focus.

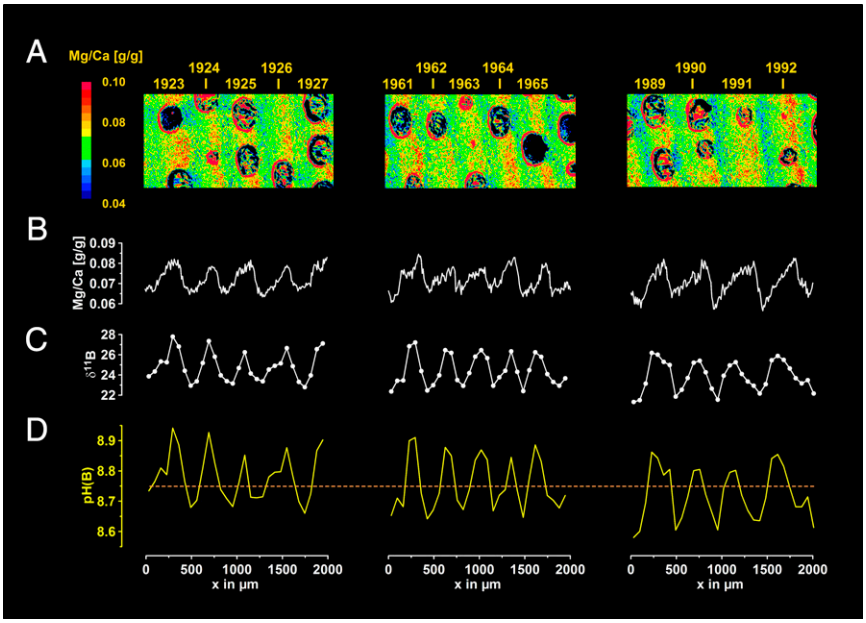

Fig. 4. Seasonal pH variability. (*A*) EMP Mg/Ca elemental maps (10 µm resolution) for the time slices (TS-1923/27, TS-1961/65, and TS-1989/92) selected for not showing any traces of skeletal destruction from grazing. "TS-years" designates the $\delta^{11}B$ time series and the time interval covered. (*B*) Mg/Ca time series obtained from *A* used for temperature calculation. (*C*) $\delta^{11}B$ time series determined via LA–MC–ICP–MS (66 µm resolution). (*D*) Internal (calcifying fluid) pH derived from $\delta^{11}B$ time series using Mg/Ca-derived temperatures to correct boric acid pK_B (for details see *SI Appendix*). Dashed line represents the mean pH (8.75) of the three time-series data.

The comparison of annual Mg/Ca and $\delta^{11}B$ peak positions in the time-series data provides a first indication of long-term temporal shifts of algal (kelp) growth season (*SI Appendix*, *S6*). Mg/Ca peaks, indicating the annual temperature maxima, show a weak temporal trend toward higher relative positions within the annual growth band, possibly due to an increase in spring/summer growth. An opposite trend toward lower relative positions is observed for $\delta^{11}B$ peaks representing pH, which always precede their corresponding Mg/Ca peak. The offset between $\delta^{11}B$ and Mg/Ca peaks (expressed as percentage of annual growth) changed from $10 \pm 9\%$ (TS-1923/27) to $20 \pm 11\%$ (TS-1961/65) and $39 \pm 10\%$ (TS-1989/92). This is interpreted as a long-term shift of algal (kelp) growth toward earlier times of the season in the study area. Together with the above-mentioned warming trend, our results indicate an ongoing ecosystem shift in this high-latitude ocean coastal habitat.

The detection of intraannual variability in pH caused by the seasonal uptake of CO_2 by algae (kelp) for photosynthesis applying the presented methodology enables us to reconstruct intensities and timing of the growth season influenced by parameters like light, temperature, and nutrient supply (e.g., from upwelling or volcanic ash supply) over wide temporal and spatial scales. Particularly through the use of long-lived crustose coralline algae, natural pH variability and long-term trends can be investigated in the higher latitudes, the part of the oceans showing the strongest CO_2 uptake. In combination with similar records from lower latitudes, for example, using corals or coralline algae, this will help to increase our understanding of the complex responses of marine ecosystems with respect to pH in a world of further increasing atmospheric CO_2.

Methods

Stable boron isotope analysis via LA–MC–ICP–MS was performed using two different approaches (for full technical details, see *SI Appendix*, *S3*):

i) Two-dimensional images (3×3 mm^2, 100 μm resolution) referred to as boron images B-1888/94 and B-1989/96 were acquired to evaluate the spatial distribution of $\delta^{11}B$. The growth periods covered are B-1889/94, 1888–1894 and B-1989/96, 1989–1996 (Fig. 3*A*).

ii) Time series (2 mm long, 66 μm resolution) focusing on primary calcite to evaluate the intraannual variability of $\delta^{11}B$ and to put better constraints on the long-term trend observed between B-1889/94 and B-1989/96. Three time series have been acquired for the years 1923–1927 (TS-1923/27), 1961–1965 (TS-1961/65), and 1989–1992 (TS-1989/92) (Fig. 4*C*).

To identify representative regions for LA–MC–ICP–MS boron measurements, calibrated Mg/Ca elemental maps were generated using EMP analysis, a nondestructive microchemical surface technique (technical details can be found in *SI Appendix*, *S2*). Mg/Ca data provided information for temperature reconstruction and sample chronology (for data handling, see *SI Appendix*, *S4*).

The entire sample section (about 60×12 mm^2) was first analyzed by EMP in low resolution (30 μm) (Fig. 2*A*). Based on this overview map, two sample areas (covering the last decades of the 19th and 20th century—M-1887/97, 1887–1897 and M-1988/98, 1988–1998) were selected for high-resolution EMP mapping analysis (5×5 mm^2, 5 μm resolution) (Fig. 2*B*). Within these areas, the two boron images B-1888/94 and B-1989/96 have been acquired.

Further high-resolution EMP maps cover the areas used for the boron time-series analyses, TS-1923/27, TS-1961/65, and TS-1989/92 (Fig. 4*A*), each representing at least 4–5 consecutive annual layers of undisturbed growth.

Details of the calculations used to convert $\delta^{11}B$ data into pH can be found in *SI Appendix*, *S4* (44–48). pH is expressed as total scale. All uncertainties in the text are 1 SD.

ACKNOWLEDGMENTS. The authors thank the editor and three anonymous reviewers for their constructive comments and helpful suggestions to improve the manuscript. Funding for this study was provided by the BMBF joint-project BIOACID 03F0608B, TP 3.2.4 (to J.F., T.H.H., and F.R.). J.H. was supported by National Science and Engineering Resource Council and Canadian Foundation for Climate and Atmospheric Sciences grants. Funding to collect specimens was provided by US National Science Foundation Grant PLR-1316141 (to R.S.S.).

1. Sabine CL, et al. (2004) The oceanic sink for anthropogenic CO_2. *Science* 305(5682):367–371.
2. Caldeira K, Wickett ME (2003) Oceanography: Anthropogenic carbon and ocean pH. *Nature* 425(6956):365.
3. Stocker TF, et al., eds (2013) *IPCC Climate Change 2013: The Physical Science Basis*, contribution of working group I to the Fifth Assessment Report of the Intergovernmental Panel on Climate Change (Cambridge Univ Press, Cambridge, UK).
4. Orr JC, et al. (2005) Anthropogenic ocean acidification over the twenty-first century and its impact on calcifying organisms. *Nature* 437(7059):681–686.
5. Hofmann GE, et al. (2010) The effect of ocean acidification on calcifying organisms in marine ecosystem: An organisms-to-ecosystem perspective. *Annu Rev Ecol Evol Syst* 41:127–147.
6. Kuffner IB, Andersson AJ, Jockel PL, Rodgers KS, Mackenzie FT (2008) Decreased abundance of crustose coralline algae due to ocean acidification. *Nat Geosci* 1(2):114–117.
7. Zeebe RE, Wolf-Gladrow DA (2001) *CO_2 in Seawater: Equilibrium, Kinetics, Isotopes*, Elsevier Oceanography Series 65 (Elsevier, Amsterdam), pp 346.
8. Ragazzola F, et al. (2012) Ocean acidification weakens the structural integrity of coralline algae. *Glob Change Biol* 18(9):2804–2812.
9. Martin S, Gattuso JP (2009) Response of Mediterranean coralline algae to ocean acidification and elevated temperature. *Glob Change Biol* 15(8):2089–2100.
10. Hönisch B, et al. (2012) The geological record of ocean acidification. *Science* 335(6072):1058–1063.
11. Hemming NG, Hanson GN (1992) Boron isotopic composition and concentration in modern marine carbonates. *Geochim Cosmochim Acta* 56(1):537–543.
12. Hönisch B, Hemming NG (2005) Surface ocean pH response to variations in pCO_2 through two full glacial cycles. *Earth Planet Sci Lett* 236(1-2):305–314.
13. Kasemann SA, Schmidt DN, Bijma J, Foster GL (2009) In situ boron isotope analysis in marine carbonates and its application for formaminifera and palaeo-pH. *Chem Geol* 260(1-2):138–147.
14. Foster GL, Ni Y, Haley B, Elliot T (2006) Accurate and precise isotopic measurement of sub-nanogram sized samples of foraminiferal hosted boron by total evaporation NTIMS. *Chem Geol* 230(1-2):161–174.
15. Pelejero C, et al. (2005) Preindustrial to modern interdecadal variability in coral reef pH. *Science* 309(5744):2204–2207.
16. Foster GL (2008) Seawater pH, pCO_2 and $[CO_3^{2-}]$ variations in the Caribbean Sea over the last 130 kyr: A boron isotope and B/Ca study of planktic foraminifera. *Earth Planet Sci Lett* 271(1-4):254–266.
17. Douville E, et al. (2010) Abrupt sea surface pH change at the end of the Younger Dryas in the central sub-equatorial Pacific inferred from boron isotope abundance in corals (Porites). *Biogeosci* 7(8):2445–2459.
18. Fietzke J, et al. (2010) Boron isotope ratio determination in carbonates via LA-MC-ICP-MS using soda-lime glass standards as reference material. *J Anal At Spectrom* 25(12):1953–1957.
19. Halfar J, et al. (2011) 225 years of Bering Sea climate and ecosystem dynamics revealed by coralline algal growth-increment widths. *Geology* 39(6):579–582.
20. Freiwald A, Henrich R (1994) Reefal coralline algal build-ups within the Arctic Circle: Morphology and sedimentary dynamics under extreme environmental seasonality. *Sedimentology* 41(5):963–984.
21. Foster MS (2001) Rhodoliths: Between rocks and soft places. *J Phycol* 37(5):659–667.
22. Kamenos NA, Law A (2010) Temperature controls on coralline algal skeletal growth. *J Phycol* 46(2):331–335.
23. Digby PSB (1977) Photosynthesis and respiration in the coralline algae, Clathromorphum circumscriptum and Corallina officinalis and the metabolic basis of calcification. *J Mar Biol Assoc U K* 57(4):1111–1124.
24. Halfar J, Steneck RS, Joachimski M, Kronz A, Wanamaker AD, Jr (2008) Coralline red algae as high resolution climate recorders. *Geology* 36(6):463–466.
25. Kamenos NA, Cusack M, Moore PG (2008) Coralline algae are global palaeothermometers with bi-weekly resolution. *Geochim Cosmochim Acta* 72(3):771–779.
26. Smith TM, Reynolds RW (2004) Improved extended reconstruction of SST (1854-1997). *J Clim* 17(12):2466–2477.
27. Reed RK, Stabeno PJ (1994) Flow along and across the Aleutian ridge. *J Mar Res* 52(4):639–648.
28. Reed RK, Stabeno PJ (1999) The Aleutian north slope current. *Dynamics of the Bering Sea: A Summary of Physical, Chemical, and Biological Characteristics, and a Synopsis of Research on the Bering Sea*, eds Loughlin TR, Ohtani K (North Pacific Marine Science Organization) (University of Alaska Sea Grant, Fairbanks, AK), pp 177–191.
29. Halfar J, et al. (2007) Coralline alga reveals first marine record of subarctic North Pacific climate change. *Geophys Res Lett* 34(7):1–5.
30. Adey WH (1965) The genus Clathromorphum (Corallinaceae) in the Gulf of Maine. *Hydrobiologia* 26(3):539–573.
31. Halfar J, Zack T, Kronz A, Zachos JC (2000) Growth and high-resolution paleoenvironmental signals of rohodoliths (coralline red algae): A new biogenic archive. *J Geophys Res* 105(C9):107–122.
32. Hetzinger S, et al. (2009) High-resolution Mg/Ca ratios in a coralline red alga as a proxy for Bering Sea temperature variations from 1902 to 1967. *Palaios* 24(5-6):406–412.
33. McCulloch M, et al. (2012) Resilience of cold-water sclractinian corals to ocean acidification: Boron isotopic systematics of pH and saturation state up regulation. *Geochim Cosmochim Acta* 87:21–34.

34. McCulloch M, Falter J, Trotter J, Montagna P (2012) Coral resilience to ocean acidification and global warming through pH up-regulation. *Nature Climate Change* 2(8):623–627.
35. Krief S, et al. (2010) Physiological and isotopic responses of scleractinian corals to ocean acidification. *Geochim Cosmochim Acta* 74(17):4988–5001.
36. Holcomb M, et al. (2014) Coral calcifying fluid pH dictates response to ocean acidification. *Sci Rep* 4:5207.
37. Comeau S, Carpenter RC, Edmunds PJ (2013) Coral reef calcifiers buffer their response to ocean acidification using both bicarbonate and carbonate. *Proc Biol Sci* 280(1753):20122374.
38. Takahashi T, et al. (2014) Climatological distributions of pH, pCO_2, total CO_2, alkalinity, and $CaCO_3$ saturation in the global surface ocean, and temporal changes at selected locations. *Mar Chem* 164:95–125.
39. Mann KH (1973) Seaweeds: Their productivity and strategy for growth: The role of large marine algae in coastal productivity is far more important than has been suspected. *Science* 182(4116):975–981.
40. Wilmers CC, Estes JA, Edwards M, Laidre KL, Konar B (2012) Do trophic cascades affect the storage and flux of atmospheric carbon? An analysis of sea otter and kelp forests. *Front Ecol Environ* 10(8):409–415.
41. Hofmann GE, et al. (2011) High-frequency dynamics of ocean pH: A multi-ecosystem comparison. *PLoS ONE* 6(12):e28983.
42. Doty MS, Oguri M (1956) The island mass effect. *J Cons Cons Int Explor Mer* 22: 33–37.
43. Caldeira RMA, Groom S, Miller P, Pilgrim D, Nezlin NP (2002) Sea-surface signatures of the island mass effect phenomena around Madeira Island, Northeast Atlantic. *Remote Sens Environ* 80(2):336–360.
44. Hetzinger S, et al. (2011) High-resolution analysis of trace elements in crustose coralline algae from the North Atlantic and North Pacific by laser ablation ICP-MS. *Palaeogeogr Palaeoclimatol Palaeoecol* 302(1-2):81–94.
45. Coplen TB (2011) Guidelines and recommended terms for expression of stable-isotope-ratio and gas-ratio measurement results. *Rapid Commun Mass Spectrom* 25(17): 2538–2560.
46. Klochko K, Kaufman AJ, Yao W, Byrne RH, Tossel JA (2006) Experimental measurement of boron isotope fractionation in seawater. *Earth Planet Sci Lett* 248(1-2): 276–285.
47. Dickson AG (1990) Thermodynamics of the dissociation of boric-acid in synthetic seawater from 273.15-K to 318.15-K. *Deep-Sea Res* 37(5):755–766.
48. Foster GL, Pogge von Strandmann PAE, Rae JWB (2010) Boron and magnesium isotopic composition of seawater. *Geochem Geophys Geosyst* 11:Q08015.